New Journal of Physics
The open access journal at the forefront of physics

Deutsche Physikalische Gesellschaft DPG
IOP Institute of Physics

Published in partnership with: Deutsche Physikalische Gesellschaft and the Institute of Physics

OPEN ACCESS

RECEIVED
17 February 2017

REVISED
24 March 2017

ACCEPTED FOR PUBLICATION
5 April 2017

PUBLISHED
28 April 2017

PAPER

Andreev reflection without Fermi surface alignment in high-T_c van der Waals heterostructures

Parisa Zareapour[1], Alex Hayat[1], Shu Yang F Zhao[1,5], Michael Kreshchuk[1], Zhijun Xu[2], T S Liu[2,6], G D Gu[2], Shuang Jia[3,7], Robert J Cava[3], H-Y Yang[4], Ying Ran[4] and Kenneth S Burch[4]

[1] Department of Physics and Institute for Optical Sciences, University of Toronto, 60 St George Street, Toronto, Ontario M5S 1A7, Canada
[2] Department of Condensed Matter Physics and Materials Science (CMPMS), Brookhaven National Laboratory, Upton, New York 11973, United States of America
[3] Department of Chemistry, Princeton University, Princeton, New Jersey 08544, United States of America
[4] Department of Physics, Boston College, 140 Commonwealth Avenue, Chestnut Hill, MA 02467, United States of America
[5] Present Address: Department of Physics, Harvard University, Boston MA, United States of America.
[6] Present Address: School of Chemical Engineering and Environment, North University of China, People's Republic of China.
[7] Present Address: International Center for Quantum Materials, School of Physics, Peking University, Beijing 100871, People's Republic of China.

E-mail: ks.burch@bc.edu

Keywords: high-T_c superconductors, topological materials, Andreev reflection

Abstract

We address the controversy over the proximity effect between topological materials and high-T_c superconductors. Junctions are produced between $Bi_2Sr_2CaCu_2O_{8+\delta}$ and materials with different Fermi surfaces (Bi_2Te_3 and graphite). Both cases reveal tunneling spectra that are consistent with Andreev reflection. This is confirmed by a magnetic field that shifts features via the Doppler effect. This is modeled with a single parameter that accounts for tunneling into a screening supercurrent. Thus the tunneling involves Cooper pairs crossing the heterostructure, showing that the Fermi surface mismatch does not hinder the ability to form transparent interfaces, which is accounted for by the extended Brillouin zone and different lattice symmetries.

1. Introduction

Potential novel optical devices [1, 2] and non-abelian anyons [3–8] have reinvigorated interest in the superconducting proximity effect. Various approaches to high-temperature superconducting proximity have claimed success [9–17], including the recent report of a proximity effect between $Bi_2Sr_2CaCu_2O_{8+\delta}$ and Bi_2Se_3 or Bi_2Te_3 [18, 19], via the mechanical bonding technique. Using thin films and ARPES, another group has claimed such interfaces result in an s-wave superconductor in the surface states [20]. One theoretical study has suggested that this is due to a mismatch in the crystal symmetries [21], though another finds that the d-wave channel is dominant [22]. Two other thin film/ARPES studies suggest the proximity effect is not possible due to the Fermi surface mismatch, which suppresses the interface transparency [23, 24].

We test this hypothesis with tunneling experiments on junctions between $Bi_2Sr_2CaCu_2O_{8+\delta}$ (Bi-2212) and Bi_2Te_3 or graphite in a magnetic field. These van der Waals materials are chosen as they form mechanical junctions with different Fermi surfaces. The Bi_2Te_3 is hole-doped with a Fermi surface close to the Γ point [25], whereas graphite is a semimetal with pockets close to the zone boundary (see figure 1(c)) [26]. By establishing Andreev reflection and proximity, we show that our original efforts, which focused on similar materials (Bi_2Te_3 and Bi_2Se_3), are not a special case. The ability to obtain Andreev reflection despite the Fermi surface mismatch is explained by considering the extended zone scheme, which is where the Fermi surfaces meet.

The heterostructure is probed using differential conductance (dI/dV) to look for Andreev reflection, which is the process where a quasiparticle converts into a Cooper pair and travels from the normal material into the superconductor (see figure 1(a)). Andreev reflection is responsible for the proximity effect and is a stringent test of a transparent interface [27–30]. In metals with no attractive potential, one expects [31] and observes [32] a pair amplitude that can result in a minigap, whose size depends on the device geometry and superconducting

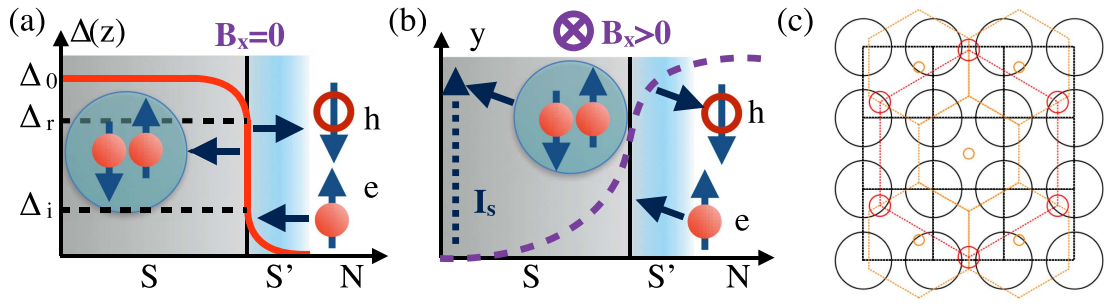

Figure 1. (a) The Andreev reflection process at the superconductor-normal interface without a magnetic field. (Red) the order parameter, Δ_0 the bulk superconducting gap, Δ_r the gap at the surface, and Δ_i the induced gap. (b) The affects of the applied magnetic field. (c) The Fermi surfaces in the extended Brillouin zone; the dotted lines are the boundaries of the zones, and the solid lines are the Fermi surfaces, with black Bi-2212, red graphite, and orange Bi_2Te_3.

phase of the contacts. In confined devices, with two superconductors separated by a normal material, Andreev reflection can produce an Andreev bound state (nABS) inside the normal region [32–36]. The nABS can ultimately lead to a supercurrent inside such devices. We do not expect the nABS to be relevant here as we form planar junctions with only one superconductor. Furthermore, since both Bi_2Te_3 and graphite have been shown to superconduct with applied pressure or doping [37, 38], they must have existing pairing potentials, and thus can hold a proximity effect without the need to invoke the nABS. As described later, the magnetic field dependence of our spectra is inconsistent with previous measurements of nABS or induced pair amplitudes without a corresponding proximity effect (i.e. a superconducting order parameter).

2. Experimental details

We measured numerous devices with either a high or low barrier. In high-barrier devices we observe tunneling spectra that are consistent with those measured in previous planar junctions, point contacts or STM experiments (see figure 2(b)) [39–46]. In addition, they are well described by an accepted theory of tunneling into the *c*-axis of a d-wave superconductor [30, 42], with the correct value of the superconducting gap (40 meV). In both Bi_2Te_3 and graphite heterostructures with low barriers, the conductance is enhanced below T_c, which is consistent with Andreev reflection in a proximity-induced region. This interpretation is further confirmed by the application of a magnetic field, which generates supercurrents. Tunneling into these supercurrents shifts the momentum of the quasiparticles and ultimately their energy. Since this only occurs for superconducting quasiparticles, the observation of the Doppler effect confirms the presence of Andreev reflection, as established in numerous theoretical and experimental works [44, 45, 47–57].

The Doppler effect manifests itself as a shift in the Andreev features to lower voltages. This is seen in Bi_2Te_3 and graphite junctions, confirming that they are not due to the normal field dependence of the material. Due to the large size of our devices and the application of the field in the *ab*-plane, we expect effectively random or no observable shift in ABS. All field-dependent spectra are well described by including the Doppler shift in a previously established model of the Andreev reflection for proximity junctions. Furthermore, no hysteresis or splitting of any features is observed, as had been seen in previous measurements of ABS due to the sign change at the 110 surface of $Bi_2Sr_2CaCu_2O_{8+\delta}$ (dABS) [40, 42]. Taken together, our results confirm the Andreev reflection between $Bi_2Sr_2CaCu_2O_{8+\delta}$ and the normal materials, implying the relative alignment of the Fermi surface is not crucial in these heterostructures. This likely occurs due to the different lattice symmetries, which allow the Fermi surfaces to overlap in the extended zone (see figure 1(c)).

To form planar junctions between the normal material and Bi-2212 ($T_c \sim 90$ K) we employed the mechanical bonding method as described in references [18, 19]. Both materials were cleaved in an inert glove box, then the Bi-2212 was placed on top of the Bi_2Te_3 or graphite, and GE varnish was applied to the corners of the Bi-2212 (figure 2(c)). Four-point transport measurements were performed at various temperatures ranging from 290 K–10 K. To further clarify the nature of the interface we performed extensive AFM on the cleaved surfaces. The Bi-2212 had extremely large, flat areas, whereas the Bi_2Te_3 and graphite produced step edges with atomically flat regions which were typically tens of microns across (figure 2(e)). Some regions showed mesas jutting out (figure 2(d)). Given the geometry of our devices, this suggests that the tunneling is along the *c*-axis of both materials, and occurs at planar junctions formed by these mesas touching the Bi-2212. The dI/dV were highly reproducible regardless of the field, temperature or voltage approach taken. To confirm that the dI/dV spectra originate from the junction, for every device we checked different sets of contacts and different combinations of them. Devices where the spectra were not reproducible between different contact sets were

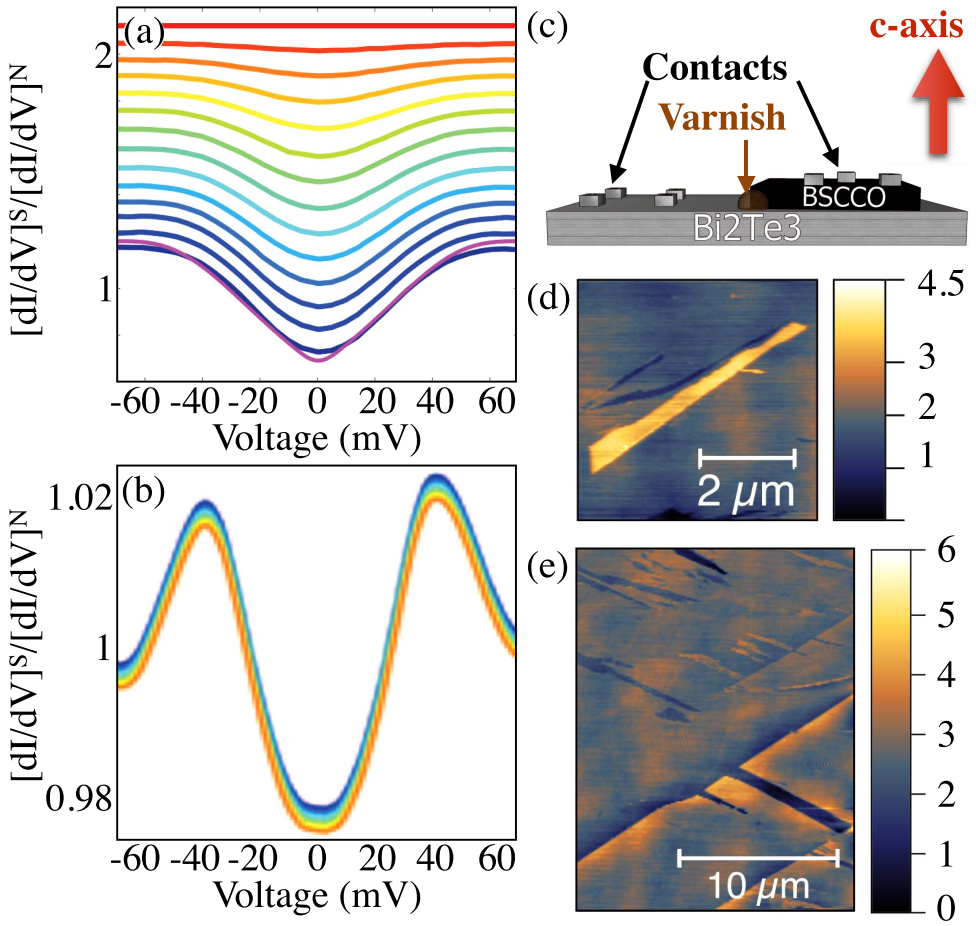

Figure 2. (a) dI/dV normalized to its value at T_c from a high-barrier Bi_2Te_3 junction. The purple line shows the fit with an energy-independent lifetime and a maximum gap of 40 meV. (b) A high-barrier junction with offsets due to extra resistance in the graphite upon applying an in-plane magnetic field every Tesla from 0 (blue) to 5 T (orange). (c) A schematic of the device indicating that the *c*-axis of the materials is normal to the interface. (d) and (e) The AFM from the cleaved surface of Bi_2Te_3 revealing atomically flat regions, with some raised mesas and step edges; the color bar indicates the height in nm.

not considered. This confirms that the tunneling directly probes the interface between the materials, whereas previous experiments probed the top surface [20, 22–24].

The features we observed might not have arisen from tunneling given the large contact area. However, it is well established that superconductivity occurs within the Cu-O plane, while the outer layers of the $Bi_2Sr_2CaCu_2O_{8+\delta}$ insulate Bi-O and Sr-O, enabling interlayer Josephson junctions and tunneling within a single crystal [39]. Thus we speculate that the Bi-O layer forms a tunnel barrier with the normal material enabling the dI/dV to provide spectra. The large contact area also suggests scattering on either side could occlude the observation of tunneling. This is not the case for our junctions, as shown by the high-barrier device (figure 2(a)). Consistent with previous experiments and the d-wave gap [39–46], we see a v-like shape at a low T that is gradually filled as the temperature is raised. Furthermore, the data is well described by the standard approach to d-wave tunneling on the *c*-axis, producing a proper gap at 40 mV [30, 41, 42]. The fit required a broadening parameter $\Gamma \approx 1 \rightarrow 4$ meV, which was much smaller than any of the features observed. This is likely due to the large mobilities of the normal materials used and the *c*-axis nature of the tunneling, reducing the likelihood of scattering.

Confirmation that none of the measured features arise from within the materials is provided by extensive measurements of various contact configurations and application of the magnetic field. Four-point and two-point measurements on only one side of the junction were independent of voltage, and the reported features were only observed when the current and voltage were measured across the interface. Two-point measurements on one side of the junction resulted in resistances $1 \rightarrow 10\ \Omega$ at low T. Swapping the current and voltage leads on the normal material only produced a slight voltage-independent offset of a few Ω, while high-barrier devices had resistances >1 kΩ and the low-barrier junctions had $dV/dI \approx 100\ \Omega$, confirming that the voltage drop primarily occurs at the interface. Further confirmation of the voltage independence of the contribution of the material is shown in figure 2(b), where we measured the response from another high-barrier junction between graphite and Bi-2212 at 10 K in various applied magnetic fields (similar results were observed with Bi_2Te_3).

Consistent with the STM measurements, we find no field dependence of the spectra [41], and a slight voltage-independent offset due to the graphite magneto-resistance.

3. Model

To understand the dI/dV from the low-barrier junctions, we review what is expected, observed in proximity devices by tunneling [18, 19, 29, 58–61] and confirmed with ARPES [62]. The superconducting order parameter is induced into the normal material by the conversion of a quasiparticle current into a supercurrent via Andreev reflection. This involves an electron crossing the interface by forming a Cooper pair, resulting in the doubling of conductance (figure 1(a)). In less transparent interfaces, the conductance at zero bias is smaller than two and the shape at finite voltage is altered [30, 60]. The width of the zero-bias feature reflects the full gap of the superconductor. However, if superconductivity is induced in the normal material, the gap of the superconductor is reduced at the surface. Thus we define an induced (Δ_i) and reduced gap (Δ_r) at the interface (figure 1(a)).

Since the Andreev reflection into the induced gap occurs in the normal material without a physical barrier, for $V < \Delta_i$ the normal quasiparticle is converted to a Cooper pair at the interface between the normal and induced superconducting regions, at which point it can easily travel into the superconductor. Thus dI/dV ($V \leqslant \Delta_i$) will resemble what is expected for a low-barrier contact. For $\Delta_i < V < \Delta_r$ the normal quasiparticles now make it all the way to the real barrier, where they will Andreev reflect into the reduced gap region of the superconductor—albeit with a finite barrier—producing peaks at $V \approx \Delta_r$. If the region over which the reduction in the gap of the superconductor is small, then normal quasiparticles may also tunnel into the full gap of the superconductor (Δ_0), resulting in a peak in dI/dV at $V = \Delta_0$. It should be noted that in a real system, one must also account for the evolution of the wavefunctions and potential multiple reflections. Numerical calculations in s-wave [63] and in d-wave [64] proximity junctions confirm this picture. Thus the induced and reduced gaps produce Andreev features in the dI/dV that are tell-tale signs of the proximity effect [18, 19, 29, 58–62].

The observed features are reproduced by modifying a standard approach to tunneling into d-wave superconductors [30, 60, 63, 64]. Specifically, the differential conductance below T_c $[dI/dV]_S$, divided by the normal state conductance $[dI/dV]_N$ is given by the half-sphere integration over the solid angle Ω:

$$\sigma(E) = \frac{\int d\Omega \cos\theta_N \sigma_S(E)}{\int d\Omega \sigma_N \cos\theta_N} \tag{1}$$

where E is the quasiparticle energy and θ is the incidence angle (relative to the interface normal) in the normal material, σ_N is the conductance from normal to normal material with the same geometry, and

$$\sigma_S = \frac{\sigma_N(1 + \sigma_N|k_+|^2 + (\sigma_N - 1)|k_-k_+|^2)}{1 + (\sigma_N - 1)|k_-k_+|^2 \exp(i\phi_- - i\phi_+)} \tag{2}$$

where $k_\pm = \frac{E - \sqrt{|E^2| - |\Delta_\pm^2|}}{|\Delta_\pm|}$ and $\Delta_\pm = |\Delta_\pm|\exp(i\phi_\pm)$, and the electron-like and hole-like quasiparticles are effective pair potentials with the corresponding phases $i\phi_\pm$. For simplicity we assume that the induced order has the same d-wave k-dependence as the bulk Bi-2212. Thus for all calculations we set the hole-like and the electron-like quasiparticles transmitted into the superconductor to experience the same effective pair potentials. In particular, for the c-axis tunneling that is relevant here, they have similar dependence on the azimuthal angle α in the ab-plane $\Delta_+ = \Delta_- = \Delta_0 \cos(2\alpha)$. Scattering-induced energy broadening (Γ) is included in the calculation by adding an imaginary term to the energy of the quasiparticles. The real part of the resulting σ_S then gives the differential conductance (G) with broadening from the normal material included via the Γ term ($G(\Delta, \Gamma, V) = \mathrm{Re}[\sigma]$, where V is the applied bias) [65, 66].

The total Andreev reflection spectrum at a zero magnetic field is obtained by calculating the reflection and the transmission in the proximity region, followed by reflection at the interface between the two materials [67]. Incoming quasiparticles with energies smaller than Δ_i, Andreev-reflect at the first interface. This gives rise to a $G(\Delta_i, \Gamma, V)$, which is expected to consist of a central peak with a width that is typically much smaller than the bulk gap of Bi-2212, corresponding to the induced gap in the normal material ($G(\Delta_i, \Gamma, V)$). Quasiparticles with higher energies do not Andreev-reflect off the first interface, and instead transmit as normal particles. The transmission rate is 2-$G(\Delta_i, \Gamma, V)$, where the 2 accounts for the fact that Andreev reflection involves a charge of $-2e$ due to the conversion of two normal quasiparticles into a Cooper pair (figure 1 B). Quasiparticles with energies between Δ_i and Δ_r Andreev-reflect at the second interface and give rise to a term $G(\Delta_r, \Gamma, V)$. We expect $G(\Delta_r, \Gamma, V)$ to consist of peaks at an energy that is smaller than the bulk gap of Bi-2212 (Δ_r), due to the suppression of superconductivity at the interface. Lastly, an additional term is included, $G(\Delta_0, \Gamma, V)$, which can arise due to the inhomogeneity in the tunnel junction (a few high-barrier junctions in parallel with the low-

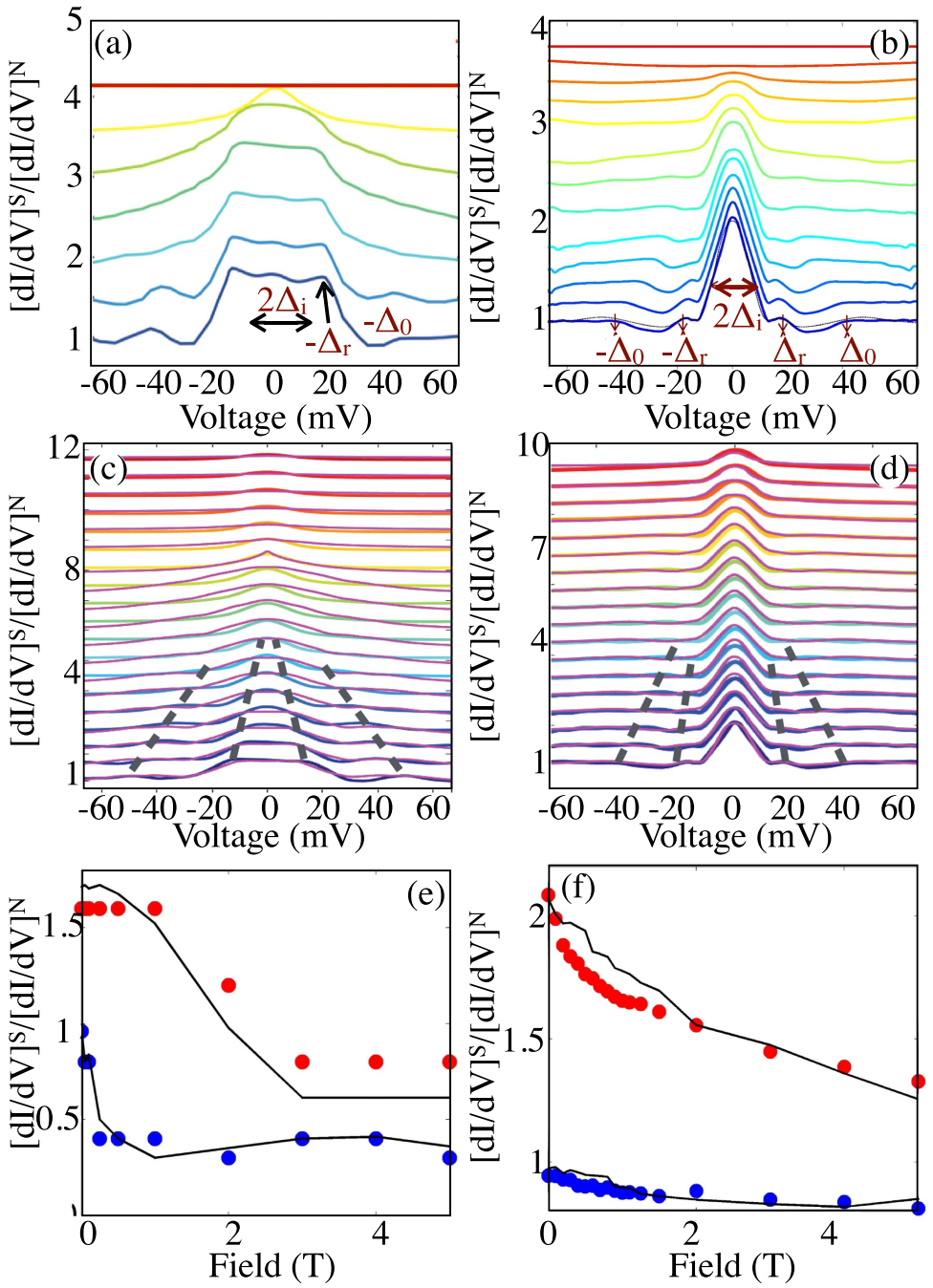

Figure 3. (a), (c), (e) Bi-2212/ Bi_2Te_3 and (b), (d), (f) Bi-2212/graphite. (a)–(b) Offset, the normalized dI/dV of Bi_2Te_3 (75 K, 60 K, 50 K, 40 K, 30 K and 20 K), and graphite data every 10 K from T_c to 70 K, then every 5 K till 25 K, and finally 11 K. The three peaks due to the Andreev reflection into induced (Δ_i), reduced (Δ_r) and full gaps (Δ_0). (c)–(d) The dI/dV in the parallel magnetic field, with the fits shown in purple. For Bi_2Te_3 the fields are 0.05, 0.1, 0.25, 0.5, 1, 2, 3, 4, 5, 6, 7 and 7.5 T, while for graphite they are every 0.1 T till 1 T, then 1.1, 1.25, 1.5, 2, 3, 4 and 5 T; the features shift due to the Doppler effect. (e)–(f) The dots show the measured data at 43 mV (blue) and 0 mV (red) versus the field; the black lines are fits with Doppler.

barrier proximity junction) or from a small reduced gap region. The total dI/dV is calculated using $G_{\text{total}} = f_1 \times [G(\Delta_i, \Gamma, V) + (2 - G(\Delta_i, \Gamma, V))G(\Delta_r, \Gamma, V)] + f_2 \times G(\Delta_0, \Gamma, V)$. The parameters f_1 and f_2 account for the different relative areas of the proximity and high-barrier junctions. Specifically, the two types of junctions are in parallel such that their total conductance is equal to their relative volume fractions ($f_{1,2}$) times their intrinsic conductivity. The calculated spectra in this model with the barrier strength (Z), scattering-induced energy broadening (Γ), and the superconducting gap (Δ) used as fit parameters, show excellent agreement with the experimental conductance measurements (purple lines in figures 2(a), 3(c) and (d)).

Typically we find $f_1 \approx 0.85$, 5 meV $\leqslant \Delta_{\text{induced}} \leqslant$ 10 meV, 15 meV $\leqslant \Delta_{\text{reduced}} \leqslant$ 35 meV, 1 meV $\leqslant \Gamma \leqslant$ 4 meV, $Z_{\text{low}} \approx 0.1$ and $Z_{\text{high}} \geqslant 3$.

4. Results and discussion

The temperature-dependent dI/dV of the Bi-2212/Bi_2Te_3 junctions is shown in figure 3(a). The dI/dV, when normalized to T_c, reveals a zero-bias peak that emerges just below T_c and eventually evolves into three features at low temperature. The first is an Andreev reflection peak near the zero-bias, whose width is much smaller than the full gap of Bi-2212 (labeled Δ_i). This feature could be a dABS [30, 40, 42]. However, at low T, the feature reaches an amplitude of nearly twice the normal state conductance, which is consistent with standard Andreev reflection. Furthermore, *ab*-plane tunneling only reveals a narrow peak at zero-bias and at the full gap at Bi-2212 (Δ_0). The full gap is also seen in our data, and its temperature dependence matches well what is observed in high-barrier devices (figure 2) and the established trends for cuprates. Another peak in our data (Δ_r) around 20 meV also approaches 2. Taken together, these three peaks are consistent with the proximity effect (figure 1(a)). Specifically, we expect perfect Andreev reflection since there is effectively no barrier between the normal material and the induced superconductor, while the inverse proximity effect reduces the size of the gap at the interface resulting in a peak at the reduced (Δ_r) gap, and at the full gap (Δ_0). We find similar spectra and temperature dependence from a low-barrier device with graphite as the normal material (figure 3(b)). The fact that we observe a zero-bias feature with a height of nearly 2 and a full gap at 40 meV, adds confidence that these features arise from Andreev reflection and do not require the Fermi surface of the normal material to directly overlap that of the superconductor.

To confirm the results of these features from Andreev reflection, we use an in-plane magnetic field $B = \nabla \times A(r)$, which dramatically affects the ABS but causes little magneto-resistance in the normal materials. The superconducting order parameter will acquire an inhomogeneous phase $\left(\phi(r) = -2\frac{\pi}{\phi_0}\int A(r')\mathrm{d}r'\right)$, where ϕ_0 is the flux quantum. This produces a diamagnetic screening current where the Cooper pairs acquire the momentum $\hbar k_s = \nabla\phi$. Since Andreev reflection involves tunneling into this supercurrent, they are Doppler shifted by $E_D = -\frac{\hbar^2 k_\perp k_s}{2m_e}$, where $k_\perp$ is the transverse wavenumber. Thus the magnetic fields shift the Andreev reflection features by $\Delta E = -v_F P_S \sin\theta$ (where v_F, P_S, and θ are the normal material Fermi velocity, Cooper pair momentum, and the angle between the electron trajectory and magnetic field). The superfluid momentum (P_S) is linearly proportional to B and includes a geometric factor whose exact size is difficult to estimate in proximity devices [40, 42, 44, 45, 47–50, 53, 54, 56]. Thus for features involving the tunneling of Cooper pairs, we expect to include into the calculation a Doppler shift: $\Delta E = D|B|$, where D is a constant and $|B|$ is the magnetic field strength. As discussed in detail later, care must be taken, as the magnetic field changes the energy dependence of the probability of Andreev tunneling. Thus the Doppler shift cannot be directly applied to the positions in the voltage of the features in dI/dV.

In studies of dABS in Bi-2212, applying a magnetic field splits and/or suppresses the zero-bias peak due to the Doppler effect, except when the field is aligned in the *ab*-plane [40, 42]. Alternatively, in S/N/S or N/S/N one can observe nABS due to multiple Andreev reflections between the interfaces. These nABS, which can play a crucial role in the proximity effect and supercurrents, have an energy defined by the phase difference across the confined region, Δ_0 and the transparency of the barrier [33]. In a confined structure with an induced pair amplitude, the resulting minigap was reduced by a *perpendicular* magnetic field [32], as expected from the theory [31], due to ϕ between the superconducting contacts.

The situation in our devices is quite different from what is typically observed in low-T_c structures. Due to the large $H_{c2} \approx 90$ T, we do not expect significant shifts in Δ_0 for the fields applied here ($\leqslant$7.5 T) [68]. However, if nABS emerge due to the small mesas seen in AFM, then their energy will be periodic in the magnetic field as the phase winds through 2π [33–36]. Using the cross-sectional area of our $Bi_2Sr_2CaCu_2O_{8+\delta}$ ($\approx 10^{-7}$m^2) or accounting for the small size of the mesas, we find that the features will reach zero energy at $B \approx 10^{-5}$ T. Thus if our features arise from nABS, their shifts with the field will essentially be random for the sizes of the fields we apply. Furthermore, nABS should only appear below the induced gap. Hence the feature at 40 meV should result from tunnelling into the full gap of $Bi_2Sr_2CaCu_2O_{8+\delta}$, whereas the features at lower energy could be nABS. As such, while the field may tune the zero-bias peak and the peak at Δ_r, the full gap will not be affected.

In figures 3(c) and (d), we show the dI/dV spectra at 6.5 K with a magnetic field. The size of the dI/dV at zero-bias and 43 mV is shown in figures 3(e) and (f), revealing the systematic suppression of the spectra, suggesting this may be the result of dABS. However, the full gap, reduced gap and width of the induced gap features all move to a zero-bias upon applying the magnetic field. This provides strong evidence against the ABS as the full gap (Δ_0) should be field-independent, as seen in high-barrier junctions (figure 2(b)). Thus we attribute the magnetic-field-induced changes to the Doppler effect.

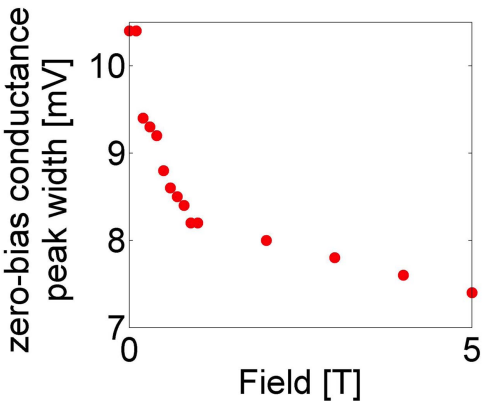

Figure 4. The width of the induced gap in graphite at 11 K for various applied fields.

This is confirmed by including the Doppler effect in our calculation of the *c*-axis conductance spectra using the formalism developed for anisotropic superconductors [30]. As described in [18, 19], we modified this formalism to include contributions from the induced, reduced and fully gapped regions. A proper theoretical approach would self-consistently calculate the gap and account for potential multiple reflections due to the gradual change in the gap. However, since we do not investigate confined structures, and our minimal model captures our results, we believe it is appropriate to investigate the effects of the magnetic field. Once the zero-field spectra are captured by our model, we follow the established procedure for the Doppler effect by calculating the Andreev reflection probability $a(\tilde{E})$ with $\tilde{E} = E + \Delta E$. The entire field dependence is reproduced using only the Doppler factor $D = 0.4$ for Bi_2Te_3 and $D = 0.2$ for graphite. The resulting dI/dV and their values at fixed bias are shown in figures 3(c $\rightarrow$ f). Despite the linear dependence of the Doppler shift on the field, its effect on the tunneling conductance is non-trivial as it enters indirectly through the probability of Andreev reflection. Thus as expected from equation (2), changes in dI/dV at fixed voltages with applied magnetic field can be non-trivial. Despite the difficulty of reproducing dI/dV with only one fitting parameter (as opposed to the peak position), we observe an excellent agreement. This confirms that the field dependence of the tunneling is governed by Andreev reflection and the Doppler effect.

Before closing, let us discuss some alternate possibilities. For example, Andreev bound states formed at the 110 interface between a d-wave superconductor/normal metal can create a peak at zero bias [30, 40, 43]. However, the central peak in our data is very different from that of an Andreev bound state. We observe a reduced gap as well as a central gap, in spite of the fact that the Andreev bound state only shows up as a zero-bias peak. Lastly, the Andreev bound states are expected to split by the application of a magnetic field, while the central peak (the induced gap) in our data, not only does not split, but decreases in width with the field (figure 4 (A) [40, 43].

Other bound states, such as geometrical resonances (McMillan–Rowell and Tomasch oscillations) [69, 70], can create peaks in the differential conductance spectra. However, these peaks emerge at certain voltage positions in the Andreev spectra. Tomasch oscillations are due to resonances in the superconductor and create resonance features in the dI/dV at voltages given by: $eV_n = \sqrt{(2\Delta)^2 + \left(\frac{nhv_{fS}}{2d_S}\right)^2}$, with Δ being the superconducting energy gap, v_{fS} being the Fermi velocity in the superconductor, d_S being the thickness of the superconductor, and n being the dip number. McMillan–Rowell oscillations occur due to geometrical resonances in the normal material and the voltages of the oscillatory features are linear with n ($\Delta V = \frac{hv_{fN}}{4ed_N}$), with v_{fN} being the Fermi velocity in the normal material and d_N being the thickness of the normal layer at which the reflections occur. Neither of these oscillations agree with the peaks we observe in our data. Furthermore, these oscillations typically create features at finite bias, in contrast to our data where we observe a zero-bias conductance peak [69]. Nonetheless, the magnetic field dependence of the McMillan–Rowell and Tomasch oscillations are different from our data. These bound states are expected and seen to split as well as shift by the application of a magnetic field [71].

A proximity effect along the *c*-axis of Bi-2212 seems surprising given the short coherence length. However, the proximity effect in the cuprates is governed by their low diffusion coefficient and small density of states [28]. Thus the Andreev reflection and proximity effect observed here could result from the small density of states of Bi_2Te_3/graphite, and their poor *c*-axis transport. What about the mismatch in the Fermi surfaces between Bi-2212 and the normal materials? Since the lattice symmetries of the normal materials are quite distinct from Bi-2212, the Fermi surfaces touch in the extended Brillouin zone [25, 26, 72]. This is shown in figure 1(c), where the

Fermi level of the hole-doped Bi_2Te_3 is around the Dirac point [73], and the graphite is of ABAB stacking [74]. This argument holds for a wide range of Fermi levels.

Strong similarities between Bi_2Te_3 and graphite devices may suggest that our results are intrinsic to Bi-2212. For example, the junctions could lead to strain that produces mechanical breaks. Indeed, some devices have sharp features in the dI/dV as seen in the point contact [75]. These result from reaching the critical current in the inhomogeneous superconductor. However, such devices did not show the features reported here, and the sharp peaks were suppressed much faster in the applied magnetic field than expected from the Doppler. Furthermore, the Andreev features only appear in measurements performed across the interface.

Acknowledgments

The work at the University of Toronto was supported by the Natural Sciences and Engineering Research Council of Canada, the Canadian Foundation for Innovation, and the Ontario Ministry for Innovation. KSB acknowledges support from the National Science Foundation (grant DMR-1410846). The work at Brookhaven National Laboratory (BNL) was supported by DOE under contract no. DE-AC02-98CH10886. The crystal growth at Princeton was supported by the US National Science Foundation, grant number DMR-0819860.

References

[1] Suemune I *et al* 2006 Superconductor-based quantum-dot light-emitting diodes: role of Cooper pairs in generating entangled photon pairs *Japan. J. Appl. Phys.* **45** 9264–71
[2] Hayat A, Kee H-Y, Burch K S and Steinberg A M 2014 Cooper-pair-based photon entanglement without isolated emitters *Phys. Rev.* B **89** 094508
[3] Oreg Y, Refael G and von Oppen F 2010 Helical liquids and Majorana bound states in quantum wires *Phys. Rev. Lett.* **105** 177002
[4] Linder J, Tanaka Y, Yokoyama T, Sudbø A and Nagaosa N 2010 Unconventional superconductivity on a topological insulator *Phys. Rev. Lett.* **104** 067001
[5] Ivanov D A 2000 Non-abelian statistics of half-quantum vortices in p-wave superconductors arXiv.org
[6] Fu L and Kane C L 2009 Probing neutral Majorana fermion edge modes with charge transport *Phys. Rev. Lett.* **102** 216403
[7] Beenakker C W J 2011 Search for Majorana fermions in superconductors arXiv.org
[8] Kitaev A Y 2007 Unpaired Majorana fermions in quantum wires *Phys.-Usp.* **44** 131
[9] Decca R S, Drew H D, Osquiguil E, Maiorov B and Guimpel J 2000 Anomalous proximity effect in underdoped $YBa_2Cu_3O_{6+x}$ Josephson junctions *Phys. Rev. Lett.* **85** 3708–11
[10] Tarutani Y, Fukazawa T, Kabasawa U, Tsukamoto A, Hiratani M and Takagi K 1991 Superconducting characteristics of a planar-type $HoBa_2Cu_3O_{7x}$ $La_{1.5}Ba_{1.5}Cu_3O_{7y}HoBa_2Cu_3O_{7x}$ junction *Appl. Phys. Lett.* **58** 2707
[11] Bozovic I, Logvenov G, Verhoeven M A, Caputo P, Goldobin E and Beasley M R 2004 Giant proximity effect in cuprate superconductors *Phys. Rev. Lett.* **93** 157002
[12] Kabasawa U, Tarutani Y, Fukazawa T, Tsukamoto A, Hiratani M and Takagi K 1991 *Electrical Characteristics of* $HoBa_2Cu_3O_{7-x}$-$La_{1.5}Ba_{1.5}Cu_3O_{7-y}$-$HoBa_2Cu_3O_{7-x}$ *Junctions with Planar-type Structures Japan. J. Appl. Phys.* **30** 1670 (Part 1, No. 8)
[13] Sharoni A, Asulin I, Koren G and Millo Proximity O 2004 Effect in gold-coated $YBa_2Cu_3O_{7-\delta}$ films studied by scanning tunneling spectroscopy *Phys. Rev. Lett.* **92** 017003
[14] Kalcheim Y, Kirzhner G, An Koren T and Millo O 2011 Long-range proximity effect in $La_{2/3}Ca_{1/3}MnO_3$/(100)$YBa_2Cu_3O_{7+\delta}$ ferromagnet/superconductor bilayers: evidence for induced triplet superconductivity in the ferromagnet *Phys. Rev.* B **83** 064510
[15] Fridman I, Gunawan L, Botton G A and Wei J Y T 2011 Scanning tunneling spectroscopy study of *c*-axis proximity effect in epitaxial bilayer manganite/cuprate thin films *Phys. Rev.* B **84** 104522
[16] Sefrioui Z, Arias D, Peña V, Villegas J E, Varela M, Prieto P, León C, Martinez J L and Santamaria J 2003 Ferromagnetic/superconducting proximity effect in $La_{0.7}Ca_{0.3}MnO_3/YBa_2Cu_3O_{7-\delta}$ superlattices *Phys. Rev.* B **67** 214511
[17] Golod T, Rydh A, Krasnov V M, Marozau, Uribe-Laverde M A, Satapathy D K, Wagner T and Bernhard C 2013 High bias anomaly in $yba_2cu_3o_{7x}/lamno_{3+\delta}/yba_2cu_3o_{7x}$ superconductor/ferromagnetic insulator/superconductor junctions: evidence for a long-range superconducting proximity effect through the conduction band of a ferromagnetic insulator *Phys. Rev.* B **87** 134520
[18] Zareapour P *et al* 2012 Proximity-induced high-temperature superconductivity in the topological insulators Bi_2Se_3 and Bi_2Te_3 *Nat. Commun.* **3** 1056–8
[19] Zareapour P *et al* 2014 Evidence for a new excitation at the interface between a high-T_c superconductor and a topological insulator *Phys. Rev.* B **90** 241106
[20] Wang E *et al* 2013 Fully gapped topological surface states in Bi_2Se_3 films induced by a d-wave high-temperature superconductor *Nat. Phys.* **9** 621–5
[21] Li Z-X, Chan C and Yao H 2015 Realizing Majorana zero modes by proximity effect between topological insulators and d-wave high-temperature superconductors *Phys. Rev.* B **91** 235143
[22] Li W-J, Chao S-P and Lee T-K 2016 Theoretical study of large proximity-induced s-wave-like pairing from a d-wave superconductor *Phys. Rev.* B **93** 035140
[23] Yilmaz T, Pletikosić I, Weber A P, Sadowski J T, Gu G D, Caruso A N, Sinkovic B and Valla T 2014 Absence of a proximity effect for a thin-films of a Bi_2Se_3 topological insulator grown on top of a $Bi_2Sr_2CaCu_2O_{8+\delta}$ cuprate superconductor *Phys. Rev. Lett.* **113** 067003
[24] Xu S-Y, Liu C, Richardella A, Belopolski I, Alidoust N, Neupane M, Bian G, Samarth N and Hasan M Z 2014 Fermi-level electronic structure of a topological-insulator/cuprate-superconductor based heterostructure in the superconducting proximity effect regime *Phys. Rev.* B **90** 085128
[25] Cava R J, Ji H, Fuccillo M K, Gibson Q D and Hor Y S 2013 Crystal structure and chemistry of topological insulators *J. Mater. Chem.* C **1** 3176–89
[26] Neto A H C, Guinea F, Peres N M R, Novoselov K S and Geim A K 2009 The electronic properties of graphene *Rev. Mod. Phys.* **81** 109
[27] Pannetier B and Courtois H 2000 Andreev reflection and proximity effect *J. Low Temp. Phys.* **118** 599

[28] Deutscher G and Simon R W 1991 On the proximity effect between normal metals and cuprate superconductors *J. Appl. Phys.* **69** 4137
[29] Klapwijk T M 2004 Proximity effect from an Andreev perspective *J. Supercond.* **17** 593–611
[30] Kashiwaya S, Tanaka Y, Koyanagi M and Kajimura K 1996 Theory for tunneling spectroscopy of anisotropic superconductors *Phys. Rev.* B **53** 2667
[31] Belzig W, Wilhelm F K, Bruder C, Schön G and Zaikin A D 1999 Quasiclassical Green's function approach to mesoscopic superconductivity *Superlattices Microstruct.* **25** 1251–88
[32] le Sueur H, Joyez P, Pothier H, Urbina C and Esteve D 2008 Phase controlled superconducting proximity effect probed by tunneling spectroscopy *Phys. Rev. Lett.* **100** 197002–4
[33] Tkachov G and Hankiewicz E M 2013 Helical Andreev bound states and superconducting Klein tunneling in topological insulator Josephson junctions *Phys. Rev.* **88** (7)
[34] Dirks T, Hughes T L, Lal S, Uchoa B, Chen Y-F, Chialvo C, Goldbart P M and Mason N 2011 Transport through Andreev bound states in a graphene quantum dot *Nat. Phys.* **7** 386–90
[35] Pillet J-D, Quay C H L, Morfin P, Bena C, Yeyati A L and Joyez P 2010 Andreev bound states in supercurrent-carrying carbon nanotubes revealed *Nat. Phys.* **6** 965–9
[36] Stehno M P, Orlyanchik V, Nugroho C D, Ghaemi P, Brahlek M, Koirala N, Oh S and van Harlingen D J 2016 Signature of a topological phase transition in the Josephson supercurrent through a topological insulator *Phys. Rev.* B **93** 035307
[37] Zhang J L *et al* 2011 Pressure-induced superconductivity in topological parent compound Bi_2Te_3 *Proc. Natl Acad. Sci.* **108** 24–8
[38] Hannay N B, Geballe T H, Matthias B T, Andres K, Schmidt P and MacNair D 1965 Superconductivity in graphitic compounds *Phys. Rev. Lett.* **14** 225
[39] Suzuki M, Hamatani T, Anagawa K and Watanabe T 2012 Evolution of interlayer tunneling spectra and superfluid density with doping in $Bi_2Sr_2CaCu_2O_{8+\delta}$ *Phys. Rev.* B **85** 214529
[40] Greene *et al* 2003 Planar tunneling spectroscopy of high-temperature superconductors: Andreev bound states and broken symmetries *Physica* **387** 7–7
[41] Pan S H, Hudson E W, Gupta A K, Ng K-W, Eisaki H, Uchida S and Davis J C 2000 STM studies of the electronic structure of vortex cores in $Bi_2Sr_2CaCu_2O_{8+\delta}$ *Phys. Rev. Lett.* **85** 1536–9
[42] Deutscher G 2005 Andreev-Saint-James reflections: a probe of cuprate superconductors *Rev. Mod. Phys.* **77** 109
[43] Aubin H, Greene L, Jian S and Hinks D 2002 Andreev bound states at the onset of phase coherence in $Bi_2Sr_2CaCu_2O_{8+\delta}$ *Phys. Rev. Lett.* **89** 177001
[44] Morozov N, Bulaevskii L N, Maley M P, Latyshev Y I and Yamashita T 2000 Quasiparticle and Cooper pair tunneling in the vortex state of $Bi_2Sr_2CaCu_2O_{8+\delta}$ *Phys. Rev.* B **62** R14681–4
[45] Dagan Y, Krupke R and Deutscher G 2000 [110] tunneling under applied magnetic fields into $Y_1Ba_2Cu_3O_7$: possible evidence for a field-induced id_{xy} gap component *Europhys. lett.* **51** 116
[46] Bae M H, Choi J H, Lee H J and Park K S 2006 Superconducting and pseudogap states studied by using interlayer tunneling spectroscopy on $Bi_2Sr_2CaCu_2O_8$ single crystals *J. Korean Phys. Soc.* **48** 1017–21
[47] Tkachov G and Fal'ko V 2004 Magnetic field influence on the proximity effect in semiconductor-superconductor hybrid structures and their thermal conductance *Phys. Rev.* B **69** 092503
[48] Rohlfing F, Tkachov G, Otto F, Richter K, Weiss D, Borghs G and Strunk C 2009 Doppler shift in Andreev reflection from a moving superconducting condensate in Nb/InAs Josephson junctions *Phys. Rev.* B **80** 220507
[49] Tkachov G and Richter K 2005 Andreev magnetotransport in low-dimensional proximity structures: spin-dependent conductance enhancement *Phys. Rev.* B **71** 094517
[50] Tkachov G 2005 Nonmetallic thermal transport in low-dimensional proximity structures with partially preserved time-reversal symmetry in a magnetic field *Physica* **417** 127–40
[51] Kohen A, Proslier T, Cren T, Noat Y, Sacks W, Berger H and Roditchev D 2006 Probing the superfluid velocity with a superconducting tip: the Doppler shift effect *Phys. Rev. Lett.* **97** 027001
[52] Fridman I, Kloc C, Petrovic C and Wei J Y T 2011 Lateral imaging of the superconducting vortex lattice using Doppler-modulated scanning tunneling microscopy *Appl. Phys. Lett.* **99** (19)
[53] Chesca B, Seifried M, Dahm T, Schopohl N, Koelle D, Kleiner R and Tsukada A 2005 Observation of Andreev bound states in bicrystal grain-boundary Josephson junctions of the electron-doped superconductor $La_{2-x}Ce_xCuO_{4-y}$ *Phys. Rev.* B **71** 104504
[54] Park W K, Sarrao J L, Thompson J D and Greene L H 2008 Andreev reflection in heavy-fermion superconductors and order parameter symmetry in $CeCoIn_5$ *Phys. Rev. Lett.* **100** 177001
[55] Tanaka Y, Tanuma Y, Kuroki K and Kashiwaya S 2003 Doppler shift of zero energy Andreev bound state *Proc. of the 23rd International Conf. on Low Temperature Physics: Physica* **329-333** 1444–5
[56] Leibovitch G, Beck R, Dagan Y, Hacohen S and Deutscher G 2008 Field-induced nodal order parameter in the tunneling spectrum of $YBa_2Cu_3O_{7-x}$ superconductor *Phys. Rev.* B **77** 094522
[57] Jankó B 1999 Theory of scanning tunneling spectroscopy of magnetic-field-induced discrete nodal states in a d-wave superconductor *Phys. Rev. Lett.* **82** 4703–6
[58] Wolf E L and Arnold G B 1982 Proximity electron tunneling spectroscopy *Phys. Rep.* **91** 31–102
[59] Van Son P C, van Kempen H and Wyder P 1987 New method to study the proximity effect at the normal-metal-superconductor interface *Phys. Rev. Lett.* **59** 2226
[60] Blonder G E, Tinkham M and Klapwijk T M 1982 Transition from metallic to tunneling regimes in superconducting microconstrictions: excess current, charge imbalance, and supercurrent conversion *Phys. Rev.* **25** 4515–32
[61] Nishino T, Hatano M, Hasegawa H, Kure T and Murai F 1990 Carrier reflection at the superconductor-semiconductor boundary observed using a coplanar-point-contact injector *Phys. Rev.* B **41** (10)
[62] Xu S-Y *et al* 2014 Momentum-space imaging of Cooper pairing in a half-Dirac-gas topological superconductor *Nat. Phys.* **10** 943–50
[63] Van Son P C, Van Kempen H and Wyder P 1988 Andreev reflection and geometrical resonance effects for a gradual variation of the pair potential near the normal-metal-superconductor interface *Phys. Rev.* **37** 5015–23
[64] Zareapour P, Xu J, Zhao S Y F, Jain A, Xu Z, Liu T S, Gu G D and Burch K S 2016 Modeling tunneling for the unconventional superconducting proximity effect *Supercond. Sci.Technol.* **29** 125006
[65] Dynes R C, Narayanamurti V and Garno J P 1978 Direct measurement of quasiparticle-lifetime broadening in a strong-coupled superconductor *Phys. Rev. Lett.* **41** 1509–12
[66] Pekola J P, Maisi V F, Kafanov S, Chekurov N, Kemppinen A, Pashkin Y A, Saira O P, Möttönen M and Tsai J S 2010 Environment-assisted tunneling as an origin of the Dynes density of states *Phys. Rev. Lett.* **105** 026803

[67] Strijkers G, Ji Y, Yang F Y, Chien C and Byers J M 2001 Andreev reflections at metal/superconductor point contacts: measurement and analysis *Phys. Rev.* B **63** 104510
[68] Shibauchi T, Krusin-Elbaum L, Li M, Maley M P and Kes P H 2001 Closing the pseudogap by Zeeman splitting in $Bi_2Sr_2CaCu_2O_{8+y}$ at high magnetic fields *Phys. Rev. Lett.* **86** 5763–6
[69] Shkedy L, Aronov P, Koren G and Polturak E 2004 Observation of McMillan–Rowell like oscillations in underdoped $YBa_2Cu_3O_y$ junctions oriented along the node of the d-wave order parameter *Phys. Rev.* B **69** 132507
[70] Chang H-S, Bae M-H and Lee H-J 2004 McMillan–Rowell oscillations observed in *c*-axis Au/$Bi_2Sr_2CaCu_2O_{8+\delta}$ junctions *Physica* **408-410** 618–9
[71] Shailos A, Nativel W, Kasumov A, Collet C, Ferrier M, Guéron S, Deblock R and Bouchiat H 2007 Proximity effect and multiple Andreev reflections in few-layer graphene *Europhys. Lett.* **79** 57008
[72] Yamamoto A, Onoda M, Takayama-Muromachi E, Izumi F, Ishigaki T and Asano H 1990 Rietveld analysis of the modulated structure in the superconducting oxide $Bi_2(Sr, Ca)_3Cu_2O_{8+x}$ *Phys. Rev.* B **42** 4228
[73] Hor Y S *et al* 2010 Development of ferromagnetism in the doped topological insulator $Bi_{2-x}Mn_xTe_3$ *Phys. Rev.* B **81** 195203
[74] Guinea F, Neto A H C and Peres N M R 2006 Electronic states and Landau levels in graphene stacks *Phys. Rev.* B **73** 245426
[75] Sasaki S, Kriener M, Segawa K, Yada K, Tanaka Y, Sato M and Ando Y 2011 Topological superconductivity in $Cu_xBi_2Se_3$ *Phys. Rev. Lett.* **107** 217001